Biochemical and Biophysical Research Communications 415 (2011) 691–695

Contents lists available at SciVerse ScienceDirect

Biochemical and Biophysical Research Communications

journal homepage: www.elsevier.com/locate/ybbrc

Adrenomedullin: A possible regulator of germinal vesicle breakdown

Yuuki Hiradate *, Jun Ohtake, Yumi Hoshino, Kentaro Tanemura, Eimei Sato

Laboratory of Animal Reproduction, Graduate School of Agricultural Science, Tohoku University, 1-1 Tsutsumidori-Amamiyamachi Aobaku, Sendai 981-8555, Japan

ARTICLE INFO

Article history:
Received 25 October 2011
Available online 4 November 2011

Keywords:
Adrenomedullin
Nitric oxide
Cumulus cell
GVBD
Akt

ABSTRACT

Adrenomedullin (ADM) is a multifunctional hormone that regulates processes as diverse as blood pressure and cell growth. Although expressed in the ovary, the role of ADM in this organ is not clear. In the present study, we found the expression of ADM receptor and receptor activity-modifying proteins in mouse cumulus cells but not in the oocytes. We report that germinal vesicle breakdown (GVBD), which is required for oocyte maturation, is not inhibited by ADM alone. However, ADM in the presence of the nitric oxide donor sodium nitroprusside (SNP) significantly inhibited GVBD. Furthermore, the ADM- and SNP-dependent inhibition of GVBD was abrogated by Akt blockade. Additionally, Akt expression and phosphorylation was exhibited by ADM, suggesting that Akt signaling upstream in cumulus cells is responsible. Additionally, immunohistochemical analysis revealed that ADM was localized in the granulosa cells of developed follicles, implying the possibility that ADM physiologically affects oocyte maturation *in vivo*. Our results provide the evidence that ADM can act as a GVBD regulator.

1. Introduction

In mammalian reproductive systems, oocyte meiosis is arrested within the ovarian follicles at the diplotene stage of the first meiotic prophase – this is termed as meiotic arrest. During the meiotic arrest phase, the intact nuclear membrane forms a characteristic germinal vesicle (GV) [1]. Once signal transduction is triggered by gonadotropin in cumulus cells surrounding the oocyte, GV breakdown (GVBD) is induced and meiosis is reactivated (so-called "meiotic resumption") [1]. The oocyte is then competent for fertilization until it reaches metaphase II. Oocytes isolated from immature antral follicles prior to the GV stage are incapable of completing meiosis and require further growth to acquire developmental competence [2]. This phenomenon has led to the proposal that additional processes at the GV stage are required for oocyte maturation.

Intriguingly, because mammalian oocytes cultured *in vitro* undergo spontaneous GVBD, it has been suggested that an inhibitor of meiotic resumption is present *in vivo* [3]. Several factors have been associated with GVBD inhibition, suggesting that the process is not under the control of a single "master regulator." In the present study, we have identified additional factors that can modulate meiotic resumption.

Adrenomedullin (ADM) is a pluripotent peptide isolated from a human pheochromocytoma [4] and consists of 50 amino acids in rats and mice. The ADM receptor, known as a calcitonin receptor-like receptor (CRLR), requires the co-expression of modifiers known as receptor activity modifying proteins (RAMPs) [5]. Co-expression of CRLR with RAMP-1 reconstitutes a calcitonin gene-related peptide receptor, whereas co-expression with RAMP-2 or RAMP-3 functions as an ADM receptor. ADM is expressed in many tissues and has various physiological functions, including regulation of blood pressure [4], angiogenesis [6], and cell growth [7].

Although recent studies have shown that ADM is expressed in the rat and human ovary, its role in this organ remains to be explained [8,9]. ADM stimulates cyclic guanosine monophosphate (cGMP) production via nitric oxide (NO) in various cell types [10,11], and cGMP inhibits meiotic resumption [12,13], thereby maintaining oocytes at the GV stage [14]. On the basis of these findings, we speculated that ADM might be a novel regulator of meiotic resumption. In the present study, we found that ADM can prevent spontaneous oocyte GVBD and meiotic resumption in the presence of an NO donor.

2. Materials and methods

2.1. Animals

This study was conducted in accordance with the Guide for the Care and Use of Laboratory Animals published by Tohoku University. Imprinting control region (ICR) mice were purchased from Japan SLC, Inc. (Shizuoka, Japan). Immature 20- to 23-day-old ICR mice were used for all experiments.

* Corresponding author. Fax: +81 22 717 8687.
E-mail address: hiradate@bios.tohoku.ac.jp (Y. Hiradate).

0006-291X/$ - see front matter © 2011 Elsevier Inc. All rights reserved.
doi:10.1016/j.bbrc.2011.10.139

2.2. Oocyte isolation and culture

To stimulate follicle development, each mouse was injected with 5 IU of pregnant mare's serum gonadotropin (PMSG) (Teikoku Hormone MGF, Tokyo, Japan). Cumulus–oocyte complexes (COCs) were collected 48 h after PMSG injection from large antral follicles punctured with 26-gauge needles in Leibovitz's L-15 medium (Invitrogen, Grand Island, USA) containing 0.1% polyvinyl alcohol (Sigma, St. Louis, MO). To prevent spontaneous meiotic resumption during COC collection, 300 μM dibutyryl cyclic adenosine monophosphate (dbcAMP; Sigma) was added to the medium. After washing in dbcAMP-free medium, the COCs were cultured in Waymouth's MB 752/1 medium (Invitrogen) supplemented with 5% fetal calf serum (Sankyo Kagaku, Kyoto, Japan), 0.23 mM pyruvic acid (Nacalai Tesque, Kyoto, Japan), 75 mg/L penicillin G (Meiji Seika, Tokyo, Japan), and 50 mg/L streptomycin sulfate (Meiji Seika). Approximately 20 COCs were cultured in 100-μL droplets of culture medium overlaid with paraffin liquid (Nacalai Tesque) in a humidified atmosphere of 5% CO_2 in air at 37 °C.

2.3. Chemical treatments

A 100× stock solution of ADM (Phoenix Pharmaceuticals, Burlingame, CA) and sodium nitroprusside (SNP; Sigma) was prepared in culture medium. SH-6 (Calbiochem, La Jolla, CA), U0126 (Cell Signaling Technology, Danvers, MA) and PP2 (Calbiochem) were dissolved in dimethyl sulfoxide (DMSO; Sigma). The working stocks were further diluted in culture medium to the final desired concentration in each experiment.

2.4. Assessment of GVBD occurrence

At the end of culture, cumulus cells from the COCs were removed by glass needle pipetting and scored using microscopy for the occurrence of GVBD. The percentage of oocytes at the GV stage was obtained by dividing the number of oocytes at the GV stage by the total number of cultured oocytes.

2.5. Reverse transcription polymerase chain reaction (RT-PCR)

Total RNA extraction from cumulus cells and oocytes was performed using an RNeasy Micro kit (Qiagen, Hilden, Germany) following the manufacturer's instructions. For cumulus cell and oocyte RNA extraction, approximately 100 COCs were denuded by repeated pipetting with a glass needle until the all the oocytes in the medium were aspirated. After the oocytes were separated, the cumulus cell-containing medium was transferred to 1.5-mL tubes and gently centrifuged. The cumulus cells were then obtained from the pellet. Total RNA was stored at −80 °C until use. Total RNA was reverse transcribed with SuperScript II (Invitrogen) using poly $(dT)^{12-18}$ primers (Invitrogen). The cDNAs were amplified using primers and Taq DNA polymerase (Takara Bio, Tokyo, Japan). The primer sequences of *crlr* (Genbank ID:018782), *ramp1* (Genbank ID:146522), *ramp2* (Genbank ID:019444), *ramp3* (Genbank ID:019511), and *gapdh* (Genbank ID:008084) are listed in Table 1. The PCR conditions for each treatment were as follows: denaturation at 94 °C for 5 min, 35 cycles of denaturation at 94 °C for 45 s, annealing at random temperatures (as listed in Table 1) for 45 s, extension at 72 °C for 45 s, and final extension at 72 °C for 5 min. The amplified PCR products were separated on a 2% agarose gel by electrophoresis and stained with ethidium bromide.

2.6. Immunoblotting

Protein from cumulus cells was collected from approximately 80–100 COCs cultured with 1, 10, and 100 nM of ADM for 6 h. Extraction was performed using sodium dodecyl sulfate (SDS) sample buffer, 0.5 M Tris–HCl (pH 6.8), 10% 2-mercaptoethanol, and 20% glycerol, and the proteins were separated by 12% SDS–polyacrylamide gel electrophoresis (SDS–PAGE) and transferred onto a membrane for 90 min. The membranes were immersed for 60 min in blocking solution 5% w/v skim milk for or 5% w/v bovine serum albumin (BSA) and incubated overnight at 4 °C in Tris-buffered saline and Tween 20. The antibodies used for detection were as follows: goat polyclonal anti-Akt (diluted 1:2000; Cell Signaling Technology), goat polyclonal anti-serine phosphorylated Akt (diluted 1:1000; Cell Signaling Technology) or mouse anti-α-tubulin monoclonal (diluted 1:2000; Sigma). After the incubation, the membranes were washed 3 times and incubated with horseradish peroxidase-conjugated goat anti-rabbit IgG or goat anti-mouse IgG (diluted 1:20,000; Jackson ImmunoResearch, PA) for 1 h at room temperature. The chemiluminescence was visualized using an ECL Plus system (GE Healthcare Ltd., UK).

2.7. Immunohistochemistry

Immunohistochemical analysis was performed to elucidate the localization of ADM. Ovaries were collected from 3 weeks mice. The samples were fixed in 4% formalin solution for 2 days and embedded in paraffin. The samples were divided into 5-μm-thick slices, deparaffinized, and rehydrated. After blocking the nonspecific protein binding by 5% BSA, sections were treated with rabbit anti-ADM antibody (diluted 1:500; Santa Cruz Biotechnology) overnight at 4 °C. The sections were next treated with Alexa Fluor 488-labeled goat anti-rabbit immunoglobulin antibody (diluted 1:1000; Santa Cruz) and counterstained with propidium iodide (100 μg/mL). Images of the sections were acquired using a Zeiss LSM700 confocal microscope.

2.8. Statistical analysis

Statistical differences between the means of the 2 groups were analyzed by Student's *t*-test. For the analysis of >2 groups, we used analysis of variance followed by a Bonferroni/Dunn test with STATVIEW (Abacus Concepts Inc., Berkeley, CA). Data are represented as mean ± SD and means were considered different when $P < 0.05$.

3. Results and discussion

3.1. mRNA expression of ADM receptor in cumulus cells and oocytes

Several factors are reported to have an inhibitory effect on GVBD. For example, hypoxanthine isolated from porcine follicular fluid prevents spontaneous oocyte maturation [15]. In addition, reactive oxygen species such as nitric oxide can affect oocyte maturation [16]. However, the precise mechanism of oocyte maturation has not been completely elucidated, and it is likely that other regulators have yet to be identified. This study aimed to determine whether ADM might be one such regulator.

We first investigated the expression of ADM receptor mRNA in cumulus cells and oocytes. As mentioned in the introduction, *crlr* must be co-expressed with *ramp2* or *ramp3* to create a functional ADM receptor. As shown in Fig. 1, *crlr* and *ramp1*, *ramp2*, and *ramp3* mRNAs were detected in cumulus cells but not in oocytes, suggesting that a functional ADM receptor is selectively expressed in cumulus cells. Numerous studies have indicated that cumulus cells

Table 1
Primers used in RT-PCR.

Gene	Primer sequences (5′–3′)	Product size (bp)	Annealing (°C)
crlr	Forward: TGG CTT TTC CCA CTC TGA T Reverse: TCA CAT CAC TAG ATC ATA CGT	157	53
ramp1	Forward: GAC GCT ATG GTG TGA CT Reverse: GAG TGC AGT CAT GAG CAG	249	55
ramp2	Forward: CAT GGA CTC TGT CAA GGA CTG Reverse: GTG TAT CAG GTG AGC CT	153	55
ramp3	Forward: ACC TGT CGG AGT TAC TCG Reverse: ATC AGT GTG CTT GCT GCT	262	58
gapdh	Forward: CCACTCTTCCACCTTCGATG Reverse: GAGGGAGATGCTCAGTGTTG	226	55

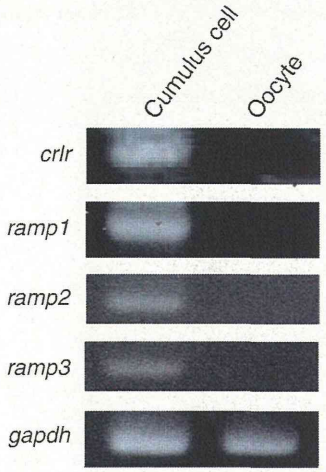

Fig. 1. mRNA expression of the ADM receptor. Reverse transcriptase polymerase chain reaction (PCR) was performed as described in Section 2 in mouse cumulus cells (A) and oocytes (B). The mRNAs of *crlr*, *ramp1*, *ramp2*, and *ramp3* were detected only in the cumulus cells and not in the oocytes. The resultant PCR products were separated on a 2% agarose gel and stained with ethidium bromide.

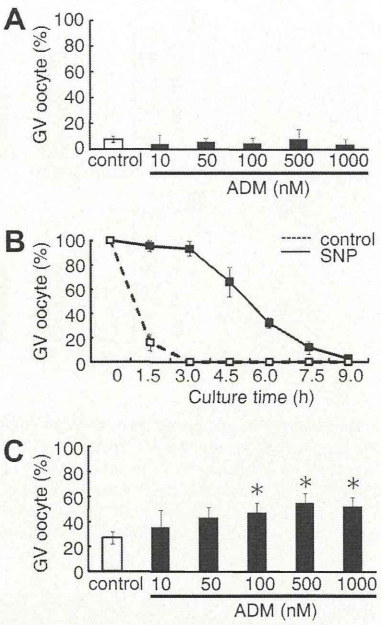

Fig. 2. Effect of ADM on germinal vesicle (GV) breakdown prevention. Cumulus–oocyte complexes (COCs) were cultured in the maturation medium with (10–1000 nM) or without ADM for 6 h (A). Time-course profiling of the percentage of oocytes at the GV stage when 1 mM of sodium nitroprusside (SNP) was added to the culture medium for 9 h (B). COCs were cultured in medium with (10–1000 nM) or without ADM containing 1 mM of SNP for 6 h (C). Values of the mean ± SD were calculated for 3 independent experiments. Data were analyzed using *t*-test. $^{*}P < 0.05$.

are important upstream regulators of GVBD since they are a source of cGMP, which maintains oocytes in meiotic arrest [13,17]. The movement of cGMP from cumulus cells to oocytes is facilitated by gap junctions formed by the tight association of these cells. This flow is present until gap junctions are closed due to luteinizing hormone activity [18].

3.2. Effect of ADM on GVBD prevention

We next examined whether ADM treatment could prevent GVBD. The addition of ADM to COCs did not influence GVBD at any concentration; in fact, no significant difference was found at 10–1000 nM (Fig. 2A). However, it is possible that, in our culture model, we lacked factors that normally co-operate with ADM to block GVBD *in vivo*. Pre-ovulatory follicles in rats contain a high-concentration milieu of nitric oxide (NO) [19]. NO produced by the nitrogen donor SNP leads to increased cGMP production by stimulating NO-dependent guanylyl cyclase activity [20]. Furthermore, cGMP production can be stimulated by ADM in various cell types [21–23]. Since cGMP is a crucial factor that controls GVBD, NO is thought to be one of the oocyte maturation inhibitors. We hypothesized that ADM works synergistically with NO to elevate cGMP levels. We therefore examined whether other known stimulators of cGMP production might cooperate with ADM in this manner.

In oocyte *in vitro* maturation, Bu et al. reported that SNP treatment induced meiotic arrest in mouse oocytes [24]. Consistent with this finding, the addition of 1 mM SNP prevented almost all oocyte GVBD 1.5 and 3 h after the start of culture and then gradually decreased (Fig. 2B). We then chose the 6-h time point to evaluate the synergistic effect of ADM in the presence of SNP because it was difficult to distinguish the effect of ADM from that of SNP in the condition in which almost all oocyte GVBD was prevented. We observed that in the presence of SNP, ADM significantly prevented oocyte GVBD at 100, 500, and 1000 nM since the frequency of oocytes at the GV stage was 47.23 ± 7.84%, 55.22 ± 7.18%, and 52.06 ± 7.47%, respectively, compared to that of control (27.05 ± 5.07%) (Fig. 2C). Taken together, these results suggest that ADM requires SNP-derived NO to inhibit GVBD. When COCs were cultured with ADM and 8-Br-cGMP, a cGMP analog, GVBD prevention was not observed (data not shown). These results imply that the additional effects of NO but not of cGMP are required for ADM to function as a meiotic inhibitor.

3.3. Effects of Akt, mitogen-activated protein kinase (MAPK), and focal adhesion kinase (FAK) inhibitor

The above results suggest that ADM can induce GVBD prevention in the presence of elevated NO and cGMP levels. Adrenomedullin exerts it effects through activation of the Akt, MAPK, and FAK signaling pathways [25]. Therefore, we examined the effects of the inhibitors of these kinases on the inhibition of GVBD by ADM. When 20 μM of Akt inhibitor SH-6 [26,27] was added in the presence of ADM, the fraction of oocytes at the GV stage was 33.96 ± 7.85%, which was significantly lower than that obtained with treatment by ADM only (56.78 ± 10.34%). This result is supported by a report that showed that induction of cGMP following

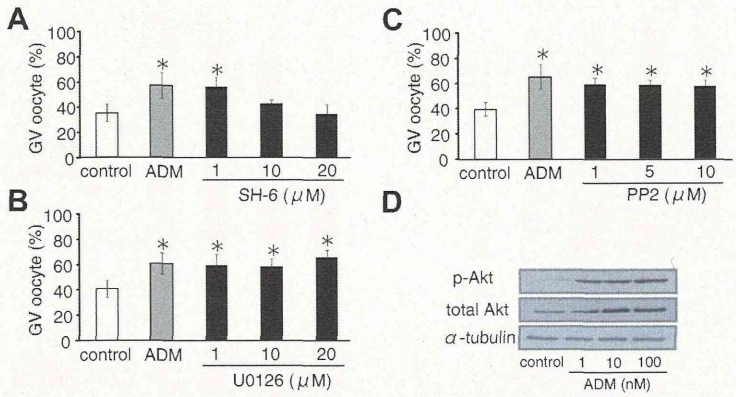

Fig. 3. ADM-induced germinal vesicle breakdown (GVBD) inhibition is regulated by Akt. Cumulus–oocyte complexes (COCs) were cultured in the presence of 1 mM sodium nitroprusside (SNP; control), SNP plus 500 nM of ADM and SNP, ADM plus SH-6 (A), U0126 (B) or PP2 (C) for 6 h. When 20 μM SH-6 was added, ADM-induced GVBD protection was significantly abolished. On the other hand, U0126 and PP2 did not affect. The inhibitors were dissolved in dimethyl sulfoxide (DMSO), and the final concentration of DMSO was <0.1% (v/v). Immunoblot detection of total Akt and phosphorylated Akt (D) in cumulus cells when different concentrations of ADM were added to the culture medium for 6 h. ADM increased both total and phosphorylated Akt. Values of the mean ± SD were calculated for 3 independent experiments and data were analyzed using one-way analysis of variance followed by a Bonferroni/Dunn test. $^{*}P < 0.05$.

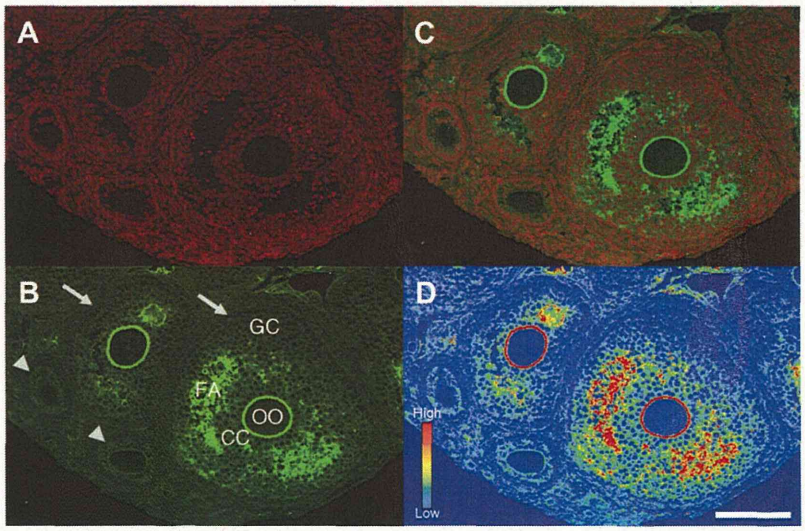

Fig. 4. Localization of ADM during follicle development. Immunostaining was performed for ADM in the ovary. The sections were treated with rabbit anti-ADM antibody and Alexa Fluor 488-labeled anti-rabbit immunoglobulin antibody. GC, CC, FA, and OO represent granulosa cell, cumulus cell, follicle antrum, and oocyte, respectively. The arrows and arrowheads represent antral follicles and pre-antral follicles, respectively. Positive staining of ADM in granulosa cells, cumulus cells and follicular antrum was observed in developed follicles. The panels show counterstaining (A), ADM (B), merge (C), and pseudo-color to show differences in fluorescence intensity (D). The scale bar represents 50 μm.

ADM treatment is mediated via activated Akt in the rat aorta [28]. In contrast, the MAPK and FAK inhibitors – U0126 [29] and PP2 [30,31], respectively – did not affect the oocyte fraction at the GV stage after ADM treatment.

The activation of Akt by ADM in cumulus cells was supported by the immunoblotting results (Figs. 3D and E). Increases in both total and phosphorylated Akt were observed, suggesting that Akt signaling and probably the NO/cGMP pathway in cumulus cells is responsible for ADM-dependent inhibition of GVBD. In contrast, we could not prove whether the ADM-induced inhibition of signal transduction facilitated GVBD because it was synonymous with cancelation of the inhibitory effect of ADM. For verifying the facilitative effect, experiments have to be performed under the "inhibited" condition, which is completely attributed to ADM. Otherwise, the condition cannot be considered "facilitated," even if overcoming the inhibitory effect was proved as long as other factors, except ADM, are needed to create the GVBD-inhibited condition.

3.4. Localization of ADM in follicles

To evaluate whether ADM is the factor that can be physiologically involved in cumulus cells and oocytes during oocyte maturation, the localization of ADM in follicles was investigated by immunohistochemical analysis. In the immunostaining analysis (Fig. 4), positive ADM staining was observed at the granulosa cells, cumulus cells and follicular antrum in the antral follicle (Fig. 4B and C). Additionally, among the antral follicles, it was shown that more strong positive signal was observed in large follicle than in small follicles (Fig. 4D), suggesting that ADM gradually accumulated in the follicular fluid as the follicle development. A study showed that cultured large follicles rather than small follicles secrete ADM *in vitro* in rats, supporting our finding, although the same study showed that the possible function of secreted ADM from the large antral follicles remains unknown [32]. Our data show that ADM is indeed a factor that can possibi1ity affect cumu-

lus cells and oocytes and involve meiotic arrest during oocyte maturation *in vivo*.

Our results show that ADM is a possible regulator of GVBD. We confirmed that ADM receptor mRNA was expressed in cumulus cells but not in oocytes and that ADM likely exerts its effects by acting on cumulus cells. The GVBD inhibitory effect of ADM was associated with the NO donor SNP, and this effect is dependent on the Akt pathway. Furthermore, positive ADM signal was detected in developed follicles. ADM may participate in the regulation of meiotic resumption *in vivo*. Further research is required to investigate the underlying mechanism(s) and the physiological role of ADM in the modulation of meiotic resumption.

Acknowledgments

This work was supported by the Japan Society for the Promotion of Science Grant to E. Sato (No. 21248032).

References

[1] R.J. Webb, F. Marshall, K. Swann, J. Carroll, Follicle-stimulating hormone induces a gap junction-dependent dynamic change in [cAMP] and protein kinase a in mammalian oocytes, Dev. Biol. 246 (2002) 441–454.
[2] J.J. Eppig, R.M. Schultz, M. O'Brien, F. Chesnel, Relationship between the developmental programs controlling nuclear and cytoplasmic maturation of mouse oocytes, Dev. Biol. 164 (1994) 1–9.
[3] G. Pincus, E.V. Enzmann, The comparative behavior of mammalian eggs in vivo and in vitro: I. The activation of ovarian eggs, J. Exp. Med. 62 (1935) 665–675.
[4] K. Kitamura, K. Kangawa, M. Kawamoto, K. Ichiki, S. Nakamura, H. Matsuo, T. Eto, Adrenomedullin: a novel hypotensive peptide isolated from human pheochromocytoma, Biochem. Biophys. Res. Commun. 192 (1993) 553–560.
[5] L.M. McLatchie, N.J. Fraser, M.J. Main, A. Wise, J. Brown, N. Thompson, R. Solari, M.G. Lee, S.M. Foord, RAMPs regulate the transport and ligand specificity of the calcitonin-receptor-like receptor, Nature 393 (1998) 333–339.
[6] M.K. Oehler, S. Hague, M.C. Rees, R. Bicknell, Adrenomedullin promotes formation of xenografted endometrial tumors by stimulation of autocrine growth and angiogenesis, Oncogene 21 (2002) 2815–2821.
[7] M.J. Miller, A. Martinez, E.J. Unsworth, C.J. Thiele, T.W. Moody, T. Elsasser, F. Cuttitta, Adrenomedullin expression in human tumor cell lines, J. Biol. Chem. 271 (1996) 22345–23351.
[8] Y.Y. Li, L. Li, I.S. Hwang, F. Tang, Coexpression of adrenomedullin and its receptors in the reproductive system of the rat: effects on steroid secretion in rat ovary, Biol. Reprod. 79 (2008) 200–208.
[9] J. Liu, R. Butzow, C. Hyden-Granskog, R. Voutilainen, Expression of adrenomedullin in human ovaries, ovarian sex cord-stromal tumors and cultured granulosa-luteal cells, Gynecol. Endocrinol. 25 (2009) 96–103.
[10] J. Dotsch, E. Schoof, H.O. Schocklmann, B. Brune, I. Knerr, R. Repp, W. Rascher, Nitric oxide increases adrenomedullin receptor function in rat mesangial cells, Kidney. Int. 61 (2002) 1707–1713.
[11] N. Ali, S.Y. Yousufzai, A.A. Abdel-Latif, Activation of particulate guanylate cyclase by adrenomedullin in cultured SV-40 transformed cat iris sphincter smooth muscle (SV-CISM-2) cells, Cell Signal. 12 (2000) 491–498.
[12] J. Tornell, H. Billig, T. Hillensjo, Resumption of rat oocyte meiosis is paralleled by a decrease in guanosine 3′, 5′-cyclic monophosphate (cGMP) and is inhibited by microinjection of cGMP, Acta Physiol. Scand. 139 (1990) 511–517.
[13] R.P. Norris, W.J. Ratzan, M. Freudzon, L.M. Mehlmann, J. Krall, M.A. Movsesian, H. Wang, H. Ke, V.O. Nikolaev, L.A. Jaffe, Cyclic GMP from the surrounding somatic cells regulates cyclic AMP and meiosis in the mouse oocyte, Development 136 (2009) 1869–1878.
[14] K. Horner, G. Livera, M. Hinckley, K. Trinh, D. Storm, M. Conti, Rodent oocytes express an active adenylyl cyclase required for meiotic arrest, Dev. Biol. 258 (2003) 385–396.
[15] S.M. Downs, D.L. Coleman, P.F. Ward-Bailey, J.J. Eppig, Hypoxanthine is the principal inhibitor of murine oocyte maturation in a low molecular weight fraction of porcine follicular fluid, Proc. Natl. Acad. Sci. USA 82 (1985) 454–458.
[16] Y. Nakamura, Y. Yamagata, N. Sugino, H. Takayama, H. Kato, Nitric oxide inhibits oocyte meiotic maturation, Biol. Reprod. 67 (2002) 1588–1592.
[17] S. Vaccari, J.L. Weeks II, M. Hsieh, F.S. Menniti, M. Conti, Cyclic GMP signaling is involved in the luteinizing hormone-dependent meiotic maturation of mouse oocytes, Biol. Reprod. 81 (2009) 595–604.
[18] R.P. Norris, M. Freudzon, L.M. Mehlmann, A.E. Cowan, A.M. Simon, D.L. Paul, P.D. Lampe, L.A. Jaffe, Luteinizing hormone causes MAP kinase-dependent phosphorylation and closure of connexin 43 gap junctions in mouse ovarian follicles: one of two paths to meiotic resumption, Development 135 (2008) 3229–3238.
[19] Y. Yamagata, Y. Nakamura, N. Sugino, A. Harada, H. Takayama, S. Kishida, H. Kato, Alterations in nitrate/nitrite and nitric oxide synthase in preovulatory follicles in gonadotropin-primed immature rat, Endocrinol. J. 49 (2002) 219–226.
[20] W.P. Arnold, C.K. Mittal, S. Katsuki, F. Murad, Nitric oxide activates guanylate cyclase and increases guanosine 3′:5′-cyclic monophosphate levels in various tissue preparations, Proc. Natl. Acad. Sci. USA 74 (1977) 3203–3207.
[21] H. Hayakawa, Y. Hirata, M. Kakoki, Y. Suzuki, H. Nishimatsu, D. Nagata, E. Suzuki, K. Kikuchi, T. Nagano, K. Kangawa, H. Matsuo, T. Sugimoto, M. Omata, Role of nitric oxide-cGMP pathway in adrenomedullin-induced vasodilation in the rat, Hypertension 33 (1999) 689–693.
[22] R. Wangensteen, A. Quesada, J. Sainz, J. Duarte, F. Vargas, A. Osuna, Role of endothelium-derived relaxing factors in adrenomedullin-induced vasodilation in the rat kidney, Eur. J. Pharmacol. 444 (2002) 97–102.
[23] C. Berenguer, F. Boudouresque, C. Dussert, L. Daniel, X. Muracciole, M. Grino, D. Rossi, K. Mabrouk, D. Figarella-Branger, P.M. Martin, L. Ouafik, Adrenomedullin, an autocrine/paracrine factor induced by androgen withdrawal, stimulates 'neuroendocrine phenotype' in LNCaP prostate tumor cells, Oncogene 27 (2008) 506–518.
[24] S. Bu, G. Xia, Y. Tao, L. Lei, B. Zhou, Dual effects of nitric oxide on meiotic maturation of mouse cumulus cell-enclosed oocytes in vitro, Mol. Cell Endocrinol. 207 (2003) 21–30.
[25] W. Kim, S.O. Moon, M.J. Sung, S.H. Kim, S. Lee, J.N. So, S.K. Park, Angiogenic role of adrenomedullin through activation of Akt, mitogen-activated protein kinase, and focal adhesion kinase in endothelial cells, FASEB J. 17 (2003) 1937–1939.
[26] A. Saskova, P. Solc, V. Baran, M. Kubelka, R.M. Schultz, J. Motlik, Aurora kinase A controls meiosis I progression in mouse oocytes, Cell Cycle 7 (2008) 2368–2376.
[27] J. Kalous, M. Kubelka, P. Solc, A. Susor, J. Motlik, AKT (protein kinase B) is implicated in meiotic maturation of porcine oocytes, Reproduction 138 (2009) 645–654.
[28] H. Nishimatsu, E. Suzuki, D. Nagata, N. Moriyama, H. Satonaka, K. Walsh, M. Sata, K. Kangawa, H. Matsuo, A. Goto, T. Kitamura, Y. Hirata, Adrenomedullin induces endothelium-dependent vasorelaxation via the phosphatidylinositol 3-kinase/Akt-dependent pathway in rat aorta, Circ. Res. 89 (2001) 63–70.
[29] H.Y. Fan, L.J. Huo, D.Y. Chen, H. Schatten, Q.Y. Sun, Protein kinase C and mitogen-activated protein kinase cascade in mouse cumulus cells: cross talk and effect on meiotic resumption of oocyte, Biol. Reprod. 70 (2004) 1178–1187.
[30] D.P. Del Re, S. Miyamoto, J.H. Brown, Focal adhesion kinase as a RhoA-activable signaling scaffold mediating Akt activation and cardiomyocyte protection, J. Biol. Chem. 283 (2008) 35622–35629.
[31] D. Hakuno, T. Takahashi, J. Lammerding, R.T. Lee, Focal adhesion kinase signaling regulates cardiogenesis of embryonic stem cells, J. Biol. Chem. 280 (2005) 39534–39544.
[32] L. Li, F. Tang, Adrenomedullin in rat follicles and corpora lutea: expression, functions and interaction with endothelin-1, Reprod. Biol. Endcrinol. 9 (2011) 111.

Entorhinal Cortex Layer III Input to the Hippocampus Is Crucial for Temporal Association Memory
Junghyup Suh *et al.*
Science **334**, 1415 (2011);
DOI: 10.1126/science.1210125

Science (print ISSN 0036-8075; online ISSN 1095-9203) is published weekly, except the last week in December, by the American Association for the Advancement of Science, 1200 New York Avenue NW, Washington, DC 20005.

The neurofeedback provided to participants was based on activation patterns only in V1/V2. However, this procedure might have induced neural activities in areas other than V1/V2, which might also contribute to VPL. To test whether other regions quantitatively contributed to VPL, we conducted two offline tests with other areas (such as V3, V4, the intraparietal sulcus, and the lateral prefrontal cortex) that have been implicated in VPL (*6*–*8*).

If the orientation-specific activation patterns in V1/V2 during the induction stage induced similar orientation-specific brain activities in other areas, the activation patterns in those areas should predict the target-orientation likelihood in V1/V2 on a trial-by-trial basis. In the first offline test, we employed a sparse linear regression method (*14*) to predict the target-orientation likelihoods in V1/V2 from activation patterns in those higher areas in each trial during the induction stage (SOM). Goodness of prediction for the target-orientation likelihood in V1/V2 by other areas, or prediction accuracies of the sparse linear regression, was evaluated by coefficients of determination, all of which were less than 5% (fig. S9A).

We conducted a second offline test to examine the possibility that the decoder simply performed poorly in higher brain areas. We examined whether accurate orientation information can be read out from each brain area when real orientation stimuli are presented in the decoder construction stage. As was done for V1/V2 during the fMRI decoder construction stage, we built a multinomial sparse logistic regression decoder to classify activation patterns into each of the three orientations (SOM). Decoding accuracies were significantly higher than chance level in all of these areas (fig. S9B, also compare fig. S9, A and B). The results of these two offline tests indicate that influences of the neurofeedback on VPL were largely confined to early visual areas such as V1/V2.

Our results indicate that the adult early visual cortex is so plastic that mere repetition of the activity pattern corresponding to a specific feature in the cortex is sufficient to cause VPL of a specific orientation, even without stimulus presentation, conscious awareness of the meaning of the neural patterns that participants induced, or knowledge of the intention of the experiment. How is the present research on VPL distinguished from previous approaches? Unit recording and brain imaging studies have successfully revealed the correlation between VPL and neural activity changes (*1*–*8*). However, these correlation studies cannot clarify cause-and-effect relationships. The studies that examined the effect of a lesion (*15*) or transcranial magnetic stimulation (TMS) (*16*, *17*) to a brain region on VPL have shown whether the examined region plays some role in VPL. However, these studies cannot clarify how particular activity patterns in the region are related to VPL. In contrast, the present decoded fMRI neurofeedback method allowed us to induce specific neural activity patterns in V1/V2, which caused VPL.

The present decoded fMRI neurofeedback method can be used to clarify cause-and-effect relationships in many functions in system neuroscience (*18*, *19*). Although previous fMRI online-feedback training is a promising technique for influencing human behaviors (*10*–*13*), as in lesion or TMS studies, it could at best reveal influences of the entire extent of an area/region on learning/memory, which is a certain limitation for neuroscientific research (*20*). In contrast, the present decoded fMRI neurofeedback method induces highly selective activity patterns within a brain region, thus allowing the investigator to influence specific functions. It can "incept" a person to acquire new learning, skills, or memory, or possibly to restore skills or knowledge that has been damaged through accident, disease, or aging, without a person's awareness of what is learned or memorized.

References and Notes

1. A. Schoups, R. Vogels, N. Qian, G. Orban, *Nature* **412**, 549 (2001).
2. Y. Yotsumoto, T. Watanabe, Y. Sasaki, *Neuron* **57**, 827 (2008).
3. T. Hua *et al.*, *Curr. Biol.* **20**, 887 (2010).
4. N. Censor, Y. Bonneh, A. Arieli, D. Sagi, *J. Vision* **9**, 1 (2009).
5. A. Karni, D. Sagi, *Nature* **365**, 250 (1993).
6. C. T. Law, J. I. Gold, *Nat. Neurosci.* **11**, 505 (2008).
7. T. Yang, J. H. Maunsell, *J. Neurosci.* **24**, 1617 (2004).
8. C. M. Lewis, A. Baldassarre, G. Committeri, G. L. Romani, M. Corbetta, *Proc. Natl. Acad. Sci. U.S.A.* **106**, 17558 (2009).
9. O. Yamashita, M. A. Sato, T. Yoshioka, F. Tong, Y. Kamitani, *Neuroimage* **42**, 1414 (2008).
10. S. Bray, S. Shimojo, J. P. O'Doherty, *J. Neurosci.* **27**, 7498 (2007).
11. A. Caria *et al.*, *Neuroimage* **35**, 1238 (2007).
12. R. C. deCharms *et al.*, *Neuroimage* **21**, 436 (2004).
13. N. Weiskopf *et al.*, *Neuroimage* **19**, 577 (2003).
14. A. Toda, H. Imamizu, M. Kawato, M. A. Sato, *Neuroimage* **54**, 892 (2011).
15. K. R. Huxlin *et al.*, *J. Neurosci.* **29**, 3981 (2009).
16. E. Corthout, B. Uttl, V. Walsh, M. Hallet, A. Cowey, *Neuroreport* **11**, 1565 (2000).
17. F. Giovannelli *et al.*, *Neuropsychologia* **48**, 1807 (2010).
18. H. R. Dinse, P. Ragert, B. Pleger, P. Schwenkreis, M. Tegenthoff, *Science* **301**, 91 (2003).
19. Y. Miyashita, *Science* **306**, 435 (2004).
20. M. Kawato, *Philos. Trans. R. Soc. London Ser. B* **363**, 2201 (2008).

Acknowledgments: This work was conducted in "Brain Machine Interface Development" under the Strategic Research Program for Brain Sciences by the Ministry of Education, Culture, Sports, Science and Technology of Japan. T.W. was partially supported by NIH grants R01 AG031941 and R01 EY015980 and Y.S. by grants R01 MH091801 and NSF 0964776. We thank J. Dobres, M. Fukuda, G. Ganesh, H. Imamizu, A. R. Seitz, and K. Tanaka for their comments on a draft of this manuscript and M. Fukuda, Y. Furukawa, S. Hirose, M. Sato, and ATR BAIC for technical assistances.

Supporting Online Material

www.sciencemag.org/cgi/content/full/334/6061/1413/DC1
Materials and Methods
Figs. S1 to S9
References (*21*–*31*)

1 August 2011; accepted 26 October 2011
10.1126/science.1212003

Entorhinal Cortex Layer III Input to the Hippocampus Is Crucial for Temporal Association Memory

Junghyup Suh,[1] Alexander J. Rivest,[1] Toshiaki Nakashiba,[1] Takashi Tominaga,[2] Susumu Tonegawa[1]*

Associating temporally discontinuous elements is crucial for the formation of episodic and working memories that depend on the hippocampal-entorhinal network. However, the neural circuits subserving these associations have remained unknown. The layer III inputs of the entorhinal cortex to the hippocampus may contribute to this process. To test this hypothesis, we generated a transgenic mouse in which these inputs are specifically inhibited. The mutant mice displayed significant impairments in spatial working-memory tasks and in the encoding phase of trace fear-conditioning. These results indicate a critical role of the entorhinal cortex layer III inputs to the hippocampus in temporal association memory.

A critical feature of episodic memory shared by some forms of working memory is the ability to associate temporally discontinuous elements, called temporal association memory (*1*–*3*). However, the neural circuits within the entorhinal cortex (EC)–hippocampus (HP) network subserving this type of association have remained unknown. The EC provides inputs to the HP via two major projections (Fig. 1A): the trisynaptic pathway (TSP) originating from EC layer II and the monosynaptic pathway (MSP) originating from EC layer III (ECIII). Studies on genetically engineered mice (*4*–*7*) and lesioned rats (*8*–*11*) have demonstrated crucial roles of the TSP in several features of episodic-memory processing, such as pattern completion (*5*–*8*) and separation (*4*, *8*). In contrast, the MSP contributions to episodic-memory processing remain poorly known. We tested the

[1]The Picower Institute for Learning and Memory, RIKEN–MIT Center for Neural Circuit Genetics, Department of Biology and Department of Brain and Cognitive Sciences, Massachusetts Institute of Technology, Cambridge, MA 02139, USA. [2]Department of Neurophysiology, Faculty of Pharmaceutical Sciences, Tokushima Bunri University, Kagawa, Japan.

*To whom correspondence should be addressed. E-mail: tonegawa@mit.edu

hypothesis that the MSP is necessary for temporal association memory.

We created a Cre transgenic mouse, pOxr1-Cre (*12*). X-gal staining and thionin staining on brain sections from the progeny of pOxr1-Cre and Rosa26 (lacZ reporter line) crosses revealed that, by 12 weeks of age, Cre-loxP recombination was restricted to superficial layers of the dorsal portion of the medial EC (MEC) and occurred sparsely in the lateral EC (LEC) (Fig. 1, B and C, and figs. S1 and S2). Immunofluorescence studies with anti–β-galactosidase (β-gal, recombination marker) (Fig. 1, D and E, and fig. S3), anti-NeuN (Fig. 1D and figs. S3 and S4), anti-PGP9.5 (fig. S3), and anti-parvalbumin (Fig. 1E and fig. S3) or anti–GAD-67 (fig. S3) indicated that recombination was mostly confined to excitatory neurons in the MEC superficial layers.

To further define the distribution of recombination within the superficial layers, we conducted neuronal tracing experiments using the retrograde tracer AlexaFluor488–cholera toxin subunit B (CTB) injected into hippocampal subregions of the progeny of pOxr1-Cre and Rosa26 crosses. CTB injection into the stratum lacunosum moleculare (SLM) of dorsal CA1 (Fig. 1F) led to colabeling of only dorsal MEC layer III (MECIII)

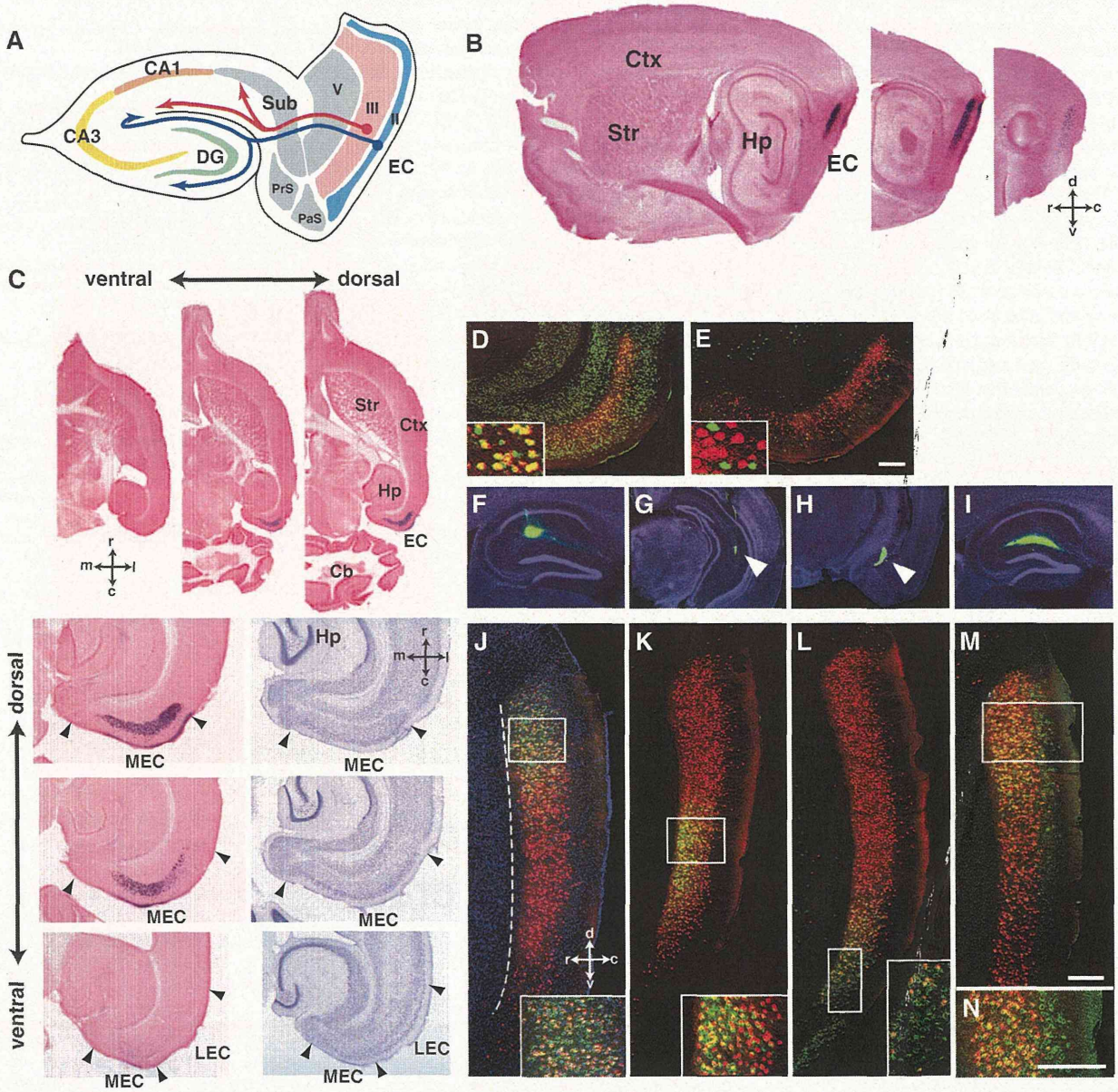

Fig. 1. Spatial specificity of Cre-loxP recombination in pOxr1-Cre transgenic mice. (**A**) Schematic of inputs from EC to HP, layer III (red, MSP) to CA1 and subiculum (Sub), and layer II (blue) to CA3 and DG. PrS, presubiculum; PaS, parasubiculum; V, layer V. (**B** and **C**) Parasagittal (B) and horizontal (C) brain sections of 12-week-old pOxr1-Cre/Rosa26 mice stained with X-gal and nuclear fast red. Adjacent sections stained with thionin (C). Arrowheads in (C) indicate MEC and LEC boundaries. Cb, cerebellum; Ctx, cortex; Str, striatum; r, rostral; c, caudal; l, lateral; m, medial. (**D** and **E**) Double immunofluorescence staining of horizontal sections of pOxr1-Cre/Rosa26 mouse with anti–β-gal [(D) and (E), red] and anti-NeuN [(D), green] or anti-parvalbumin [(E), green]. Colabeled cells in (D) are shown in yellow. (**F** to **I**) Injection sites of retrograde tracer, CTB (green), in the SLM of dorsal CA1 (F), intermediate CA1 (G), ventral CA1 (H), and the hippocampal fissure of dorsal CA1 (I). Arrowheads in (G) and (H) indicate the injection sites. (**J** to **M**) Parasagittal sections visualized with CTB-labeled cell body (green) and immunostained by anti–β-gal (red) in the EC. The dotted line denotes the lamina dissecans (J). (**N**) Magnified image from (M). Scale bars, 100 μm.

(Fig. 1J) by CTB and β-gal, whereas the injection of CTB into intermediate CA1 SLM (Fig. 1G) resulted in colabeling restricted to intermediate MECIII (Fig. 1K). In contrast, injection of the tracer into ventral CA1 SLM (Fig. 1H) led to labeling of ventral MECIII, which was poorly colabeled with β-gal (Fig. 1L). When CTB was injected into the hippocampal fissure, which covers both CA1 SLM (receives ECIII projections) and dentate gyrus (DG) stratum moleculare (receives ECII projections) (Fig. 1I) (*13*), we observed colabeling in the dorsal MECIII (Fig. 1, M and N). More importantly, there was a clear segregation of the layer II and layer III cells, confirming that recombination was primarily restricted to the MECIII (Fig. 1N and fig. S4).

To selectively inhibit synaptic transmission at the MECIII to CA1/subiculum synapses by use of the tetanus toxin light chain (TeTX), we crossed the pOxr1-Cre mouse (Tg1) with the pαCaMKII-loxP-STOP-loxP-tTA mouse (Tg2) and the tetO-TeTX mouse (Tg3) (Fig. 2A) (*5*). To examine the input-output relationship of transmission at the ECIII-CA1 synapses, we employed the fluorescent voltage-sensitive dye (VSD) imaging method (Fig. 2B and fig. S5) (*14*) on hippocampal slices prepared from the triple-transgenic mutant, MECIII-TeTX, and control mice (Tg1 x Tg2), which were raised on a doxycycline (Dox)–containing diet followed by 4 to 8 weeks of a Dox-free diet (Fig. 2, C and F). The MECIII-TeTX mice showed a significant reduction (78.4 to 95.9%) in postsynaptic fluorescence with SLM stimulation compared with controls (Fig. 2, B and D), whereas no difference of fluorescence was observed between the genotypes with stratum radiatum (SR) stimulation (Fig. 2, B and E). When hippocampal slices were prepared from MECIII-TeTX mice off Dox for 4 weeks, the postsynaptic fluorescence was reduced and matched that of the slices from MECIII-TeTX mice off Dox for 8 weeks (Fig. 2F and fig. S6). With 4 weeks of Dox withdrawal followed by 4 weeks of Dox readministration, the postsynaptic fluorescence at ECIII-CA1 synapses was restored in MECIII-TeTX mice to levels comparable to controls (Fig. 2F and fig. S6). These results demonstrate that transmission in MECIII-TeTX mice can be inhibited specifically at the MECIII-CA1 synapses in an inducible and reversible manner. Combined with the CTB tracing data from the pOxr1-Cre/Rosa26 mouse (Fig. 1, F to N), we conclude that inhibition of neuronal transmission in the MECIII-TeTX mice was restricted to synapses of the projections from the dorsal and intermediate MECIII neurons to the HP. The MECIII-TeTX mice raised on a Dox diet followed by 4-weeks of Dox withdrawal will be referred to as mutants hereafter, unless indicated otherwise.

Immunohistological analyses revealed no obvious indications of molecular and cytoarchitectural abnormalities in the EC (figs. S7, S8, and S10) and HP (figs. S7 to S9). The mutants displayed no detectable abnormalities in anxiety, motor coordination, or pain sensitivity (fig. S11). The mutants were also normal in the acquisition, recall, and consolidation of spatial reference memory (figs. S12 and S13) and in the basic properties of place fields of CA1 pyramidal neurons and interneurons (fig. S14) (*15*).

The mutants exhibited a deficit in a water-maze version of the delayed matching-to-place (DMP) task (Fig. 3A) designed to test spatial working memory, a form of temporal association memory. During early training (block 0 to block 2), the mutants showed normal escape latencies compared to controls (Fig. 3B), presumably because they were still learning the task requirements and rules (*16*, *17*). As training advanced and the platform size was reduced (blocks 3 and 4), however, the mutants' escape latencies became greater compared with the controls in runs 2 to 4. Consequently, the savings (escape latency difference between runs 1 and 2) were less for the mutants in block 3 ($t = 2.564$, $P < 0.05$) and block 4 ($t = 4.132$, $P < 0.001$) (Fig. 3C), indicating an impairment in spatial working memory.

We next subjected both genotypes to a delayed non–matching-to-place (DNMP) version of the T-maze task (Fig. 3D). The controls showed a significant improvement in performance between day 1 and day 12 (fig. S15). In contrast, the mutants were impaired in this task over the 12-day period (10 trials per day) [two-way analysis of

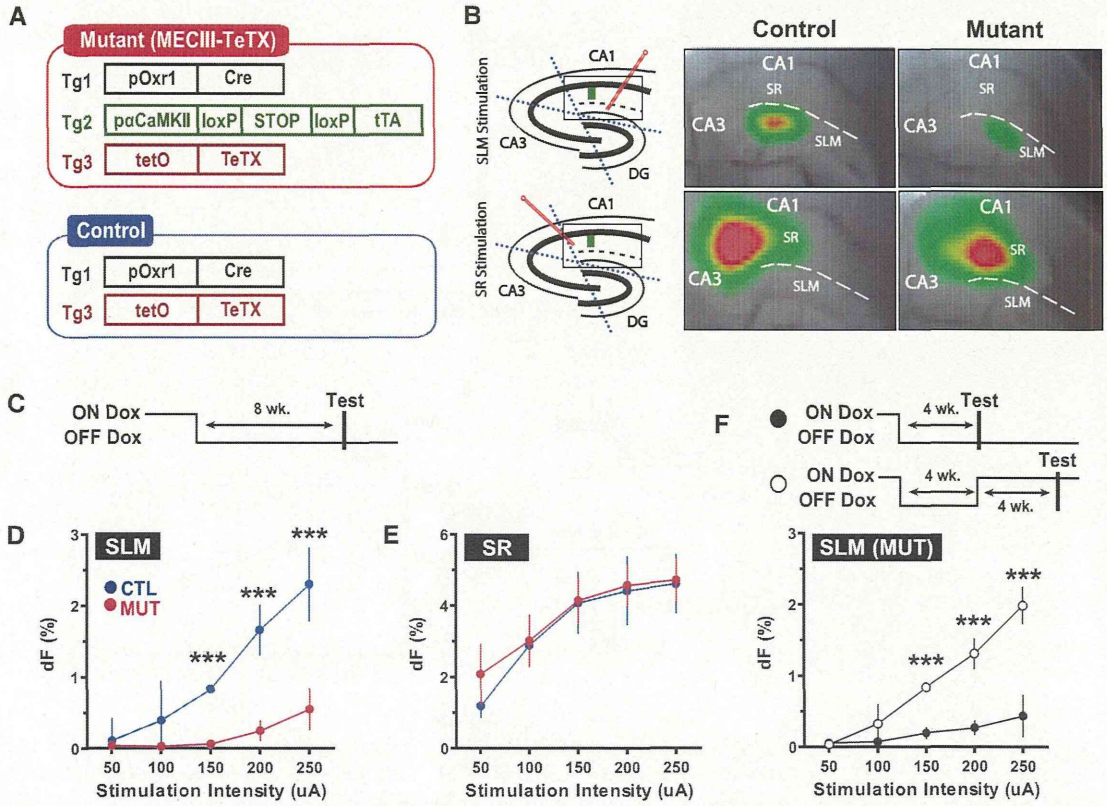

Fig. 2. Triple-transgenic MECIII-TeTX mouse (mutant) and inducible and reversible inhibition of MECIII input to CA1. (**A**) Breeding strategies for mutant and control mice. (**B**) VSD imaging of transverse hippocampal sections. A stimulating electrode (red bar) was placed in SLM or SR, and fluorescent signal was measured in SR (green square). Dotted black lines indicate knife cuts to separate CA3 and DG from CA1. Fluorescent signal changes are displayed in pseudocolor after SLM or SR stimulation in control and mutant slices. Dashed white lines indicate the boundary between SR and SLM. (**C**) Dox withdrawal schedule in VSD experiments for (D) and (E). (**D** and **E**) Input-output relationships after SLM or SR stimulation in mutant and control slices. dF, fractional changes in fluorescence. (**F**) Reversibility of the synaptic inhibition. VSD imaging was performed 4 weeks after Dox withdrawal (solid circles) and after 4 weeks of Dox withdrawal followed by 4 weeks of Dox readministration (empty circles) in mutant slices after SLM stimulation. Asterisks indicate the significance at the 0.001 level; error bars indicate SEMs.

variance: genotype, $F_{1,360} = 96.75$, $P < 0.0001$] (Fig. 3, E and F) and did not display an improvement (fig. S15), confirming the mutants' impairment in spatial working memory.

To investigate whether the MECIII input to the HP plays a role in nonspatial temporal association, we subjected the mutant and control mice to trace fear-conditioning (TFC). In this task, a tone [conditioned stimulus (CS)] must be associated with a footshock [unconditioned stimulus (US)] delivered subsequently with a 20-s time gap. The mutants froze less than controls during the training composed of three CS-US pairs (Fig. 4A). The next day, in a distinct novel chamber, mutants froze less than controls in response to tone presentation (Fig. 4A). Conversely, when the temporal gaps between the CS and US were eliminated [delay fear-conditioning (DFC)], there were no freezing differences between the two genotypes during either the acquisition or the recall phase (Fig. 4B). To investigate whether the MSP is required during the acquisition and/or recall phase in TFC, we targeted the inhibition of synaptic transmission to each of these two phases. When inhibition was targeted to the acquisition phase, mutants froze less than controls in response to tone (Fig. 4C), whereas when inhibition was targeted to the recall phase, we observed no freezing difference between the genotypes (Fig. 4D).

To further investigate the role of the EC-HP circuits in temporal association memory, we examined whether the indirect ECII input to CA1 via the TSP also played a role in TFC by using a second mutant, the CA3-TeTX mouse (*5*). These mice, in which CA3 input to CA1 is inhibited under Dox withdrawal (*5*), performed similar to controls in the TFC task (Fig. 4E).

We hypothesized that the essential function of the MECIII input to the HP in TFC may be associated with the persistent activity observed in vitro in their cells (*18*, *19*). As this activity depends on activation of the metabotropic glutamate receptor 1 (*19*) and/or cholinergic muscarinic receptors (*20*), we injected a mixture of their respective antago-

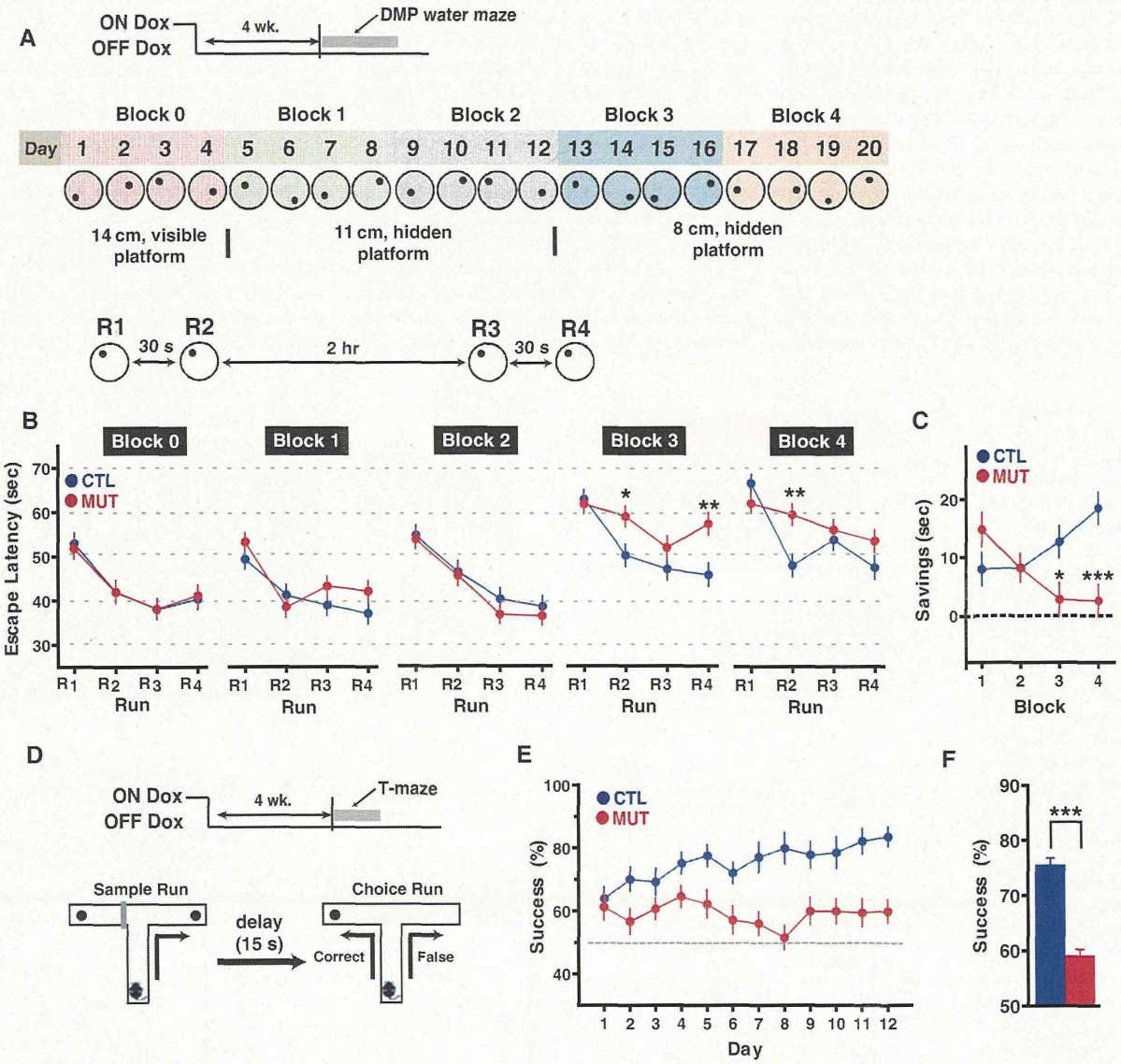

Fig. 3. Impairment of MECIII-TeTX mice in the DMP and DNMP tasks. (**A**) Protocol and Dox-schedule for a water-maze version of the DMP task. (**B**) Averaged escape latencies for run 1 (R1), R2, R3, and R4 for each 4-day block. (**C**) Averaged savings. Asterisks in (B) and (C) represent run-specific significance. (**D**) T-maze version of the DNMP task. Black dots represent rewards. (**E**) Success rate on 10 trials each day for 12 days. The gray dashed line denotes the success rate expected by a random arm selection on a choice run (50%). (**F**) Success rates averaged over 12 days. Asterisks indicate the significance at the level of 0.05 or less; error bars indicate SEMs.